Fermi National Accelerator Laboratory

FERMILAB-Pub-91/67-E
[E769]

Use of A Transition Radiation Detector in a Beam of High Energy Hadrons

D. Errede and M. Sheaff

Physics Department
Madison, Wisconsin 53706

H. Fenker, L. Lueking, and P. Mantsch

Fermi National Accelerator Laboratory
P.O. Box 500

R. Jedicke

Physics Department
Toronto, Canada M5S1A7

March 1991

* Submitted to Nucl. Instrum. Methods.

Use of A Transition Radiation Detector in a Beam of High Energy Hadrons*

D. Errede and M. Sheaff
Physics Department
University of Wisconsin
Madison, Wisconsin, 53706

H. Fenker, L. Lueking, and P. Mantsch
Fermilab
Batavia, Illinois, 60510

R. Jedicke
Physics Department
University of Toronto
Toronto, Canada M5S1A7

Abstract

A transition radiation detector (TRD) comprised of 24 identical radiator plus xenon proportional chamber assemblies was built at Fermilab and operated successfully to separate pions from protons and kaons in a 250 GeV incident hadron beam ($\gamma_\pi \sim 1800$) at rates up to, and sometimes even exceeding, 2 MHz. The detector was capable of identifying pions with efficiencies exceeding 90% and with $\leq 3\%$ percent contamination due to the nearly equally copious protons and kaons in the beam.

Introduction

It has long been known[1] that transition radiation (TR) could be used to discriminate among particle species at relativistic energies, since the intensity radiated is proportional to the Lorentz factor, γ. A more widely used technique for particle identification has been the Cerenkov counter,

but, as the particles to be identified become more and more relativistic and β approaches 1 for all species, the angular separation of the Cerenkov light from the different particle species becomes smaller than the resolution that can be achieved in such detectors. The energy at which this occurs for pions versus kaons is just above that at which pions begin to emit sufficient TR to make the transition radiation detector (TRD) a viable device[2]. Thus, there is an energy regime over which these two types of detector can be operated simultaneously for hadron identification. This was recognized at the time E769[3], a charm hadroproduction experiment at Fermilab, was conceived, and both a Differential Isochronous Self-Focusing Cerenkov Counter[4] (DISC) and a TRD were included in the 250 GeV/c hadron beam designed for the experiment. For most of the data that were recorded, the DISC was operated at a pressure such that it gave a positive tag for the incident kaons. The TRD was then used to separate pions from protons and from kaons which were not tagged by the DISC because they were outside the fiducial volume of that detector. Figure 1 demonstrates the power of the two detectors to discriminate particle species when used together in this way for beam identification. The number of DISC phototubes (of 8 total) that fired per event is shown along one axis and the number of TRD chamber planes (of 48 total) that registered a hit per event is shown along the other axis for all events on a typical E769 positive beam data tape.

Figure 2 shows the average number of TR photons expected from an incident pion, kaon, or proton as a function of particle energy for one module of the E769 TRD as calculated by a Monte Carlo program that was used extensively in planning and studying this detector[5]. The efficiency for detection of each radiated photon in the two planes of xenon-filled proportional chamber that were part of each module is included in the calculation as is the measured efficiency of 83% for the resulting signal to be above the electronics threshold of 430 mV. This corresponds to capture of a 4 keV x-ray with the chamber set to its nominal operating voltage. Since saturation is not included in the program calculations, this effect, which depends on the materials used for the radiator foils and inter-foil gaps and

the relative thicknesses of each, has been put in by hand using the formulae in Reference 6. The energy window over which separation of the common particles contained in hadron beams is feasible is seen to be of order hundreds of GeV/c, which is well-matched to the range of energies of secondary hadron beams at the Fermilab Tevatron, the highest energy accelerator in the world today.

While there are a number of experiments that have used TRD's to tag final state electrons[7,8], and, more recently, even to tag final state hadrons[9], the TRD described in this report represents the first application of a transition radiation detector to the identification of high energy hadrons in the incident beam for a running particle physics experiment.

Motivation and System Integration

The production properties of hadrons containing charm quarks has been an exciting topic of research over the past few years[10]. Especially interesting, but difficult to study because of the need to acquire not just one but several data samples with sufficient statistics, have been the differences in the production characteristics of charm particles due to differences in the quark content of the incident beam particle. E769 was designed to make a major contribution to this line of research. Exploiting a transverse energy trigger proven to enhance the charm content of accepted events[11], data for the experiment were taken in a 250 GeV/c beam containing pions, kaons, and protons of both charge signs incident on a metal foil target. By simultaneously taking positive beam data with all three beam particle species incident and identified, the experiment obtained three sets of data which can be compared directly with a minimum of experimental bias. Since the relative beam fractions were 59% pions, 35% protons, and 6% kaons, pion and proton triggers were prescaled by a large factor, up to a maximum of 30, relative to the kaon triggers to achieve data sets of more equal statistical significance.

To separate the three particle species in the positive beam, a minimum of two tagging elements was required. At 250 GeV/c it is still possible

to use the DISC Cerenkov counter, which has a resolution of $\Delta\beta \geq 4 \times 10^{-7}$, for pion/kaon separation if one can afford space for the counter itself and for the additional beam elements needed because of its special optical requirements. While the Fermilab P-East beamline for E769 had very little room to spare, it was possible, by arranging the elements compactly, to fit in the rather short DISC counter and the quadrupole magnets needed to provide a parallel beam section for it, and to have the additional 3 meters of clear space required for the TRD. A diagram showing the placement of the beamline elements in the hall upstream of the target is shown in Figure 3. With this detector arrangement, the DISC could be tuned to provide a positive tag for either protons or kaons and the TRD used to identify the pions. Additionally the DISC could be re-tuned as necessary to provide calibration data for the TRD. This was done several times during the data-taking run.

The TRD was placed in the beamline upstream of the last major bend so that particles produced by collisions with the material in the detector would be swept out of the beam upstream of the experiment target. Including the 24 radiator-chamber assemblies plus the two scintillation counters used for gating the hit register, the TRD comprises 8.3% of an interaction length and 16.9% of a radiation length, making such an arrangement necessary. This is the only major constraint on the beamline optics for a TRD. Since it makes no demands on the parallelism of the beam, and actually benefits by not being at a focus, a TRD is a very flexible device for use in beam particle identification.

Design of the TRD

Detectors

The E769 TRD is made up of 24 identical modules, each containing a radiator foil set and accompanying photon detectors, aligned along the incident beam direction. The total length of the array is 2.79 m. For this application it was decided to use the "cluster counting"[12,13] technique with

"fine sampling" chambers[2,13]. This method utilizes a detector that is highly segmented in depth so that photons are likely to be captured one-per-plane. While this necessitates the use of a relatively large number of wire planes, it allows the use of relatively simple electronics as at most one cluster needs to be reported in each plane. The fact that the detector was required to operate in a high-rate environment (~2 MHz) was further motivation for keeping the detector gaps and thus the charge collection times as small as possible.

A diagram showing the construction of one module of the TRD is shown in Figure 4, and a photograph of the entire assembly is given as Figure 5. The gas-filled detectors are proportional wire chambers derived from a proven Fermilab design[14]. They are made from anode planes containing 64 sense wires spaced at 1 mm intervals symmetrically placed between two planar cathodes which are 6.35 mm apart. The sense wires are 10.2 μm gold-plated tungsten and the cathodes are 12.7 μm mylar with 140 $\AA$ of aluminum sputtered onto both sides. This rather thin layer of aluminization actually turned out to be too thin for use in chambers exposed to such high beam rates. This was made evident by the fact that the cathodes suffered some dealuminization over the area of the beam during the highest intensity running. The means by which this problem was handled during data taking for E769 and the longer term solution for the follow-on experiment E791[15] will be discussed in detail in later sections of the paper. The chamber active area is 76 mm wide times 65 mm high. All sense wires are aligned horizontally. Two such planes make up the detector for each module. Sense wires are electrically connected in groups of four to give a total of 16 output signals per chamber plane.

Xenon was chosen as the main component of the wire chamber operating gas because of its high atomic number and correspondingly high photon absorption cross section. Two additives to it were studied as possible quenchers during the prototype tests. A mixture of 20% CO_2 in Xe was tried and rejected since it exhibited poor chamber stability at the gain required to give sufficient separation of the signals due to TR from those resulting

from ionization loss alone. The second mixture tested was pure (99.9%) Xe bubbled through methylal held at 0^o C, which results in a mixture that is approximately 90% Xe. This gas proved to be stable over a broad range of operating voltages and demonstrated a linear response to incident photons over a wide range of energies. These properties were deemed necessary enough to successful operation of the detector to warrant the extra effort required in using methylal safely.

Test bench data were taken for which a prototype chamber with the parameters described above was exposed to both an ^{55}Fe source and a dial-up radioactive source[16] which emits k_α x-rays from Cu, Rb, Mo, and Ag. Based on these prototype tests, the nominal operating voltage for the chamber cathodes was chosen so that the signals from Ag, 22.1 keV, were just under amplifier saturation. In this way, maximum gain was achieved while still maintaining a linear response over the anticipated range of transition radiation energies. That the response of the chamber to photons over the range of energies from 5.9 to 22.1 keV is linear is demonstrated in Figure 6, which plots the peak in the pulse height distribution for each of these sources as recorded in an ADC as a function of their energy. The energy of each of the sources used is also indicated along the abcissa of Figure 7 to allow direct comparison to the TR spectrum produced by the radiator stack.

The TRD modules were designed so that transition radiation photons produced in the radiators encountered a minimum amount of absorbing material before entering the sensitive region of the detector. This was achieved by flushing the radiator volume with helium, putting the highly absorbent xenon only in the chamber sensitive volume, and separating the two regions with a buffer volume purged with nitrogen. The buffer volume was necessary to keep helium from leaking through the thin aluminized mylar cathode into the xenon and altering the gain of the proportional chamber. The pressures in the three gas volumes were equalized so that there would be no bowing of the cathode foils, which would cause a gain variation across the detector plane. Because the volume of xenon in the detectors was small,

it was economically feasible to use a one-pass gas system instead of building a complicated recirculation loop.

Radiators

The total intensity, W, of transition radiation emitted in the x-ray region when a relativistic charged particle with Lorentz factor, γ, crosses an interface between two media with plasma frequencies ω_1, ω_2 grows as the difference of the plasma frequencies squared[17],

$$W = \frac{\alpha}{3} \frac{\hbar(\omega_1 - \omega_2)^2\gamma}{\omega_1 + \omega_2}.$$

The best gap material is thus vacuum, or $\omega_2 \sim 0$. The use of helium instead, for which $\hbar\omega_2$=0.28 eV, results in a reduction of only 0.3% in the radiation produced by a 250 GeV pion in a 200-foil stack of 12.7 μm polypropylene foils separated by 180 μm spacers. This includes the self-absorption of TR photons in the helium layers of the stack. Since $\omega_1 \gg \omega_2$, the intensity radiated is seen to depend linearly on ω_1, the plasma frequency of the radiator material.

For photons in the x-ray region, the radiator material acts like an electron gas, and its plasma frequency squared can be approximated as[6]:

$$\hbar^2\omega_1^2 \simeq 2(Z/A)(\rho/g\ cm^{-3})(21\ eV)^2.$$

Thus, the intensity radiated depends on the Z of the radiator material, but only as $Z^{1/2}$, while the cross section for photon absorption in the x-ray region shows a much stronger dependence, $Z^{3.5}$ (Ref 18). The best radiator material is therefore lithium[17,18], which has a relatively high plasma frequency although it is both low-Z and low-A. The relatively long radiation length means that a stack made from lithium foils will output more photons to the detector than one made from other commonly used radiator materials because fewer are self-absorbed by the foils. The relatively long interaction length means that the particles to be identified interact less frequently in

the detector material. Unfortunately, lithium is unstable and difficult to handle. A good alternative material is polypropylene, CH_2. While the addition of two hydrogen atoms to carbon results in a material that is less dense than pure carbon, this is offset by a more favorable Z to A ratio in the above formula for the plasma frequency, so that the plasma frequencies of CH_2 and pure carbon are not very different. Both the radiation length and the interaction length of polypropylene are longer than those of either pure carbon or of mylar, both of which have, however, been used successfully as radiator materials in TRD's.

It should be mentioned as part of this discussion that the optimum thickness of the radiator foils to be used with a given detector is different for the different materials and depends on the plasma frequency. This is because, at or near saturation,

$$\omega_{max} \simeq \frac{l_1 \omega_1^2}{2\pi c},$$

where ω_{max} is the frequency at which the maximum in the radiation occurs and l_1 is the foil thickness[19]. For a xenon-filled detector with cells that are shallow in depth (as in this "fine sampling" device), the optimum foil thickness is that which produces a frequency maximum in the vicinity of the xenon absorption line at 4.8 keV where the mean free path for x-ray capture is at a minimum. The thicknesses of lithium, CH_2, carbon, and mylar corresponding to ω_{max} ~4.8 keV calculated using the above expression are shown in Table I, which compares the properties of these four radiator materials. The numbers shown in the last two columns of the table are the total number of TR photons radiated, summing from 4 to 20 keV, for both a single foil (multiplied by 200) and a 200-foil stack made from each of the four materials as calculated by the Monte Carlo program for a 250 GeV pion incident. The calculations do not include absorption in the xenon detector volume. They demonstrate that, although thinner foils are optimal for the materials with higher plasma frequencies, the reduction in thickness is not large enough to offset the difference in the radiation length. While a single foil of carbon or mylar radiates more TR photons than one of lithium

or polypropylene, the self-attenuation of a 200-foil stack of these materials results in a smaller number of photons incident to the xenon detector. Using more frequent sampling, i. e., single detector planes following stacks containing fewer radiators or stacks of foils graded in thickness[20], it might be possible, however, to construct a detector that would benefit from the higher plasma frequency of these materials, so that readers interested in building TRD's in the future could consider these options.

Table I - Comparison of Various Radiator Materials

Material	Plasma Frequency	l_1 for ω_{max} =4.8 keV	l_R	single foil(x200)	200 foils
Lithium	13.85 eV	31 μm	155 cm	1.900	1.563
CH_2	21.8 eV	12.7 μm	47.9 cm	3.166	1.486
Mylar	24.8 eV	10.2 μm	28.7 cm	3.517	1.235
Carbon	26.0 eV	8.9 μm	18.8 cm	3.694	1.265

For this detector, since the time available in which to design and build it was short, approximately one year, there was not sufficient time for studying prototype radiator-chamber combinations in a test beam. It was therefore necessary to rely very heavily on the Monte Carlo simulations in determining the detector parameters. Design choices that favored ease of construction were quickly settled on and optimizations carried out within this framework using the program. These included the use of the proven chamber design, which fixed the detector cell depth at 6.35 mm, and the use of CH_2 foils for the radiator material, selecting from the various thicknesses of this material that were readily available. Figure 7 shows the program predictions for the TR produced by an incident 250 GeV pion (upper 3 curves) or kaon (lower curve) traversing one module of the TRD. What is plotted is the expected average number of TR photons per keV versus the photon energy in keV for 200-foil radiator sets made from three different thicknesses of CH_2 all with 180 μm helium-filled gaps. The calculations include detection in the two

xenon-filled detector planes. The integrated number of photons radiated by an incident beam pion between the electronics threshold of 4 keV and 20 keV is approximately the same for the 10.2 μm and 12.7 μm foils and significantly smaller for the 17.8 μm foils. Based on these results, it was decided to use the 12.7 μm foils for the radiators because the spectrum produced is somewhat harder than for the 10.2 μm foils, and thus the number of photons detected is less sensitive to gain variations in the detector. This choice does result in a somewhat larger amount of material in the incident beam. Figure 8 shows the same curve as the one shown for pions for the 12.7 μm foil set in Figure 7, but plotted on a logarithmic scale to allow comparison to another which shows the radiation produced in 200 such foils in the absence of absorption and with no requirement that the photons be captured in the xenon-filled detector. This second curve shows that the maximum frequency radiated is indeed near 4.8 keV. The foil self-absorption is responsible for the severe attenuation of the radiation at lower energies, which has the effect of shifting the detected radiation maximum to higher energy. The lengthening of the mean free path for photon absorption in xenon with increasing energy is responsible for the drop off in the radiation at energies above 8 keV when detection in the xenon is added to the simulation.

The simulations also indicated that because of increased self-absorption in the radiator stack, the addition of more foils to the sets beyond 200 did not result in a sufficient increase in the amount of radiation produced to justify the addition of the extra material to the detector. Thus, the final radiator design choice was 200 12.7 μm foils separated by 180 μm spacers made from nylon net. Large holes were cut in the center of each net to preclude attenuation of the TR photons by the non-negligible mass of the nylon. The radiators were easily fabricated as the two materials were simply cut to shape and interleaved to make the stacks. Any special preparation of the foils, e.g., stretching them over frames to assure a more uniform thickness, was ruled out as being too labor-intensive and therefore both time-consuming and expensive. As shown in Fig. 4, a stack of 200 foil-net pairs was placed inside a 10 cm diameter cylinder attached to the front face

of each detector. Appropriate gas fittings allowed the cylinder to be flushed with helium.

Electronics

A system diagram of the electronics is shown in Figure 9. The 16 sets of 4 contiguous wires in each detector plane were connected to low-noise, common-base pre-amplifiers mounted on the chamber. These hybrid pre-amplifiers are based on a circuit designed by V. Radeka[21] for use in proportional chambers operating in high-rate environments. The amplified signals are sent via short coaxial cables to 16-channel amplifier-shaper-discriminator (ASD) cards containing circuits similar in design to those used in several of the tracking detectors in the Collider Detector at Fermilab (CDF)[22]. Modifications to the basic CDF design allow the gain of each channel to be varied ~30% so system uniformity may be established and raise the range over which the discriminator thresholds may be set to that appropriate for signals due to the capture of TR photons. This is well above most signals resulting from the ionization of a beam particle in the absence of TR.

The relatively large difference in signal size between minimum ionizing particles with accompanying transition radiation (4-20 keV, peaked at ~8 keV) and those without, which is the crux of the "cluster counting" technique, is accomplished by the design of the high-speed electronics circuits. Capture of a photon causes heavy ionization in a small region in the chamber, while minimum ionizing particles deposit energy in a number of clusters along their path. Thus signals from photon capture rise more rapidly than those from ionization along a charged particle track. This difference is enhanced on the ASD cards by shaping the chamber pulses with a "pole-zero" filter, which retains the leading edges of the signals while diminishing the slower tails. The output signals resulting from photon capture as measured by exposing the chamber to an ^{55}Fe source are 26 ns wide (full width at half maximum). This is, in effect, the "resolution limit" of the electronics and, for a drift time of ~30 ns/mm corresponds to integration

of the ionization over ~1 mm of path (actually 2 mm because charge is collected simultaneously from the front and back of the chamber cell). After shaping, the signals are further amplified by a NE592N video amplifier chip (Motorola) and input to a fast LeCroy[23] time-over-threshold discriminator chip (MVL407). The discriminator thresholds are set to accept signals above those produced by a 4 keV photon, determined by extrapolating the linear fit shown in Figure 6. (Note that the pulse height in millivolts corresponding to 4 keV shown on the plot, 215 mV, is one-half the threshold set on the discriminator chip. This is because the analog output signal, which is the complementary output of the amplifier, was split into two to allow self-triggering for the source tests.) With this threshold a minimum ionizing track in the absence of TR registers a hit 8.2% of the time at the nominal chamber operating voltage. This was determined in advance of actual data-taking by exposing the prototype chamber to a ^{106}Ru source. The efficiency for TR photons to be above this threshold was also measured using the x-ray sources. It was determined to be ~83% independent of photon energy since the width as well as the peak position grows with increasing energy.

The 16 ECL discriminator outputs from each ASD card were input to one of 4 16-input logic circuits on a LeCroy[23] 4564 CAMAC module, which was configured to perform a logical OR. The resulting 48 logic signals (one per detector plane) were sent both to a LeCroy[23] 4448 CAMAC latch for readout as part of the experiment data for each event and to a summing circuit which provided an analog level proportional to the number of planes reporting a signal above threshold. This analog signal was included so that TRD information could be used in a fast trigger decision. Gating for the latch and the sum was derived from the coincidence of scintillation counters placed at either end of the TRD assembly. The gate width was set wide enough (~120 ns) to comfortably allow for the maximum electron drift time in the chamber, since photon capture may occur anywhere in the chamber cell.

Shaped and amplified signals were extracted from the ASD cards using

the analog outputs for use in special calibration runs. These signals were split into two to allow them to be routed both to a separate discriminator set to a threshold of ~100 mV, which was used as a trigger for these data, and to analog-to-digital converters (ADC's) which allowed examination of the full spectrum of chamber signals. ^{55}Fe radioactive sources were attached to each detector module to provide a continuous source of approximately monoenergetic photons. The pulse heights from these sources recorded in the ADC's during these calibration runs were used to monitor the gain of each cell so that the cathode voltages could be set to assure that all chambers were operating at the same gain.

Results

The data recorded on an event-by-event basis for use in the physics analysis of the experiment were the latch bits indicating which of the 48 planes of wire chambers had signals above the 4 keV threshold. Figures 10a) and 10b) show the distributions in the number of planes that fired per event for events with beam particles identified by the Cerenkov counter as protons and as pions, respectively. These data were taken during a second type of calibration run which differed from standard data runs only in that the DISC pressure was set to tag protons or pions in order to study the performance of the TRD. The distributions show a clear difference in the response of the detector to these two particle species. Figure 10c) shows the DISC-tagged data for a typical data run for which the DISC pressure was set to tag kaons. This data run was taken at approximately the same time as the two calibration runs. While the TRD response to kaons is seen to be almost the same as its response to protons at 250 GeV, the kaons do emit some TR, enough to raise the average plane count per event by about one plane. This was expected based on the Monte Carlo studies as shown by the kaon curve in Figure 7.

It was found necessary to apply a cut in selecting events for these distributions. As discussed above, the TRD latch gate was made wide enough to assure sufficient time for the collection of all TR photon signals associated

with a beam particle regardless of where the photon was captured within the chamber cell. Xenon is a relatively slow gas, and thus this gate was long, ~120 ns, which encompasses approximately 6 accelerator rf buckets. Since the beam had less than perfect time structure and was operating at a few MHz, there was a significant probability that more than one beam particle would pass through the detector during one gate. For these events the TRD plane count was artificially increased by hits due to the additional particle so that the plane count could not be used for tagging. Therefore, a veto circuit was implemented to negate a trigger whenever there was another beam particle within a 150 ns time window. This reduced the number of poorly tagged events, but did not eliminate them altogether. Most of the remaining such events were removed from our data by making a cut at greater than 9 on the number of clustered hits in the 8 planes of proportional chambers used for tracking the beam particles, which were downstream of the TRD past the string of bending magnets. The TRD plane counts for events surviving this cut are what is shown in Figure 10. The fraction of total events removed by the multiple-beam veto plus cut was a strong function of beam intensity and beam structure. This loss of data was occasionally as large as 25% at beam intensities of $\geq$2 MHz.

Careful examination of the proton data reveals that even after the cut on the number of hits in the proportional chambers, there remains a small number of events extending out to high plane counts. These can not be accomodated in the predicted distribution for proton events generated by using the average hit probability per plane and binomial statistics. It is unlikely that they are due to misidentification in the DISC, since the proton peak is well separated from both kaons and pions in the pressure curves. Thus, they are presumed to be events containing a second track which traversed the TRD but was outside the time gate or active volume of the beam tracking chambers. The distribution of these high plane count events appears to be the same as that of the events which fall above the cut on hits in the proportional chambers, which makes this interpretation plausible. These events represent the only significant contamination to the pion data at

high plane counts, which is the reason for the constant ~2% contamination independent of the cut on number of planes above 10 in the data shown in Table II. A neglible contamination, ~.1%, is expected from the same background source for kaons incident, i. e., a kaon not tagged due to DISC inefficiency which is accompanied by an extra beam particle.

Table II shows the efficiency for selection of either pions or protons and the background for each due to contamination by the other as a function of a cut on the number of TRD planes registering a hit. The experimental distributions shown in Figures 10a) and 10b), were used to determine the numbers shown in the columns marked "Expt.". The relative beam fractions for events selected using the global transverse energy (E_t) trigger, which was the main experiment trigger, have been folded into the calculations of the contaminations. Also shown in the table are the efficiencies and contaminations determined by making the same cuts on the functions used to fit these calibration tape distributions using the fitting procedure to be described below. The numbers determined using the fitting functions, which appear in the columns labeled "Fit", are seen to be in excellent agreement with those determined directly from the distributions. Since the DISC-tagged proton events containing a second track can not be discerned from pion events in the fits, a systematic uncertainty of 2% must be added to the errors in the efficiencies and contaminations calculated using the fitting procedures.

Table II - TRD Performance

Pions

# of TRD Planes That Fired	Pion Efficiency		Proton Contamination	
	Expt.	Fit	Expt.	Fit
≥ 8	.946	.948	4.13%	4.07%
≥ 10	.868	.868	2.23%	2.19%
≥ 12	.733	.730	1.75%	1.75%

Protons

# of TRD Planes That Fired	Proton Efficiency		Pion Contamination	
	Expt.	Fit	Expt.	Fit
< 6	.875	.875	2.00%	1.82%
< 7	.934	.929	3.26%	3.14%
< 8	.962	.957	5.48%	5.28%

The distributions shown in Figures 10a) and 10b) are not well fit using the most obvious choice of functions motivated by physics considerations. Naively, one would expect to fit the proton distribution using a single binomial function with the number of planes with hits, n, out of 48 total planes, determined using the hit probability per plane due to ionization loss alone. The pions would be expected to require the convolution of two binomials with different plane hit probabilities, one for the 24 front planes and another for the 24 rear planes in the array, since there are fewer remaining TR

photons to be detected in the downstream chamber of the pair. The experimental distributions proved to be somewhat broader than the above simple fits would allow. The peak due to each particle type can be adequately fit with a function that is the sum of two binomials, each computed over 48 total planes with different plane hit probabilities. The broadening of the distributions that makes it necessary to add a second binomial in the fits is attributed in large part to a reduction in chamber gain for incident beam particles near the beam centroid due to space charge effects. This explanation is motivated by a clear trend for the pion peak to broaden toward the lower plane count side at higher beam intensity. Further confirmation of this effect is the fact that the DISC tagged proton and pion data, which are tightly collimated and therefore near the beam centroid, have peaks which are shifted toward lower plane counts and also are narrower than pion and proton peaks in untagged distributions from data runs taken at about the same time.

Figure 11 shows the TRD plane count distribution for all E_t triggered events from a typical positive beam data tape for which the incident beam particle was not identified by the DISC to be a kaon. The curve shown is the best fit to this distribution using four binomials. The fit is normalized to contain the same number of events as the experimental distribution. There are six parameters in the fit, the plane hit probability for each of the four binomial functions used and the relative contribution of the two binomial functions summed to fit each of the two main peaks. The relative fraction of events in the two main peaks is fixed to be 50.7% for the proton peak and 49.3% for the pion peak for the fit to all data tapes. These numbers were determined by performing a preliminary fit to a number of data runs allowing the relative fraction to float. While the majority of events in the first peak are protons, an admixture of approximately 5-6% kaons is estimated by using the relative fractions of the three different species in the incident beam, the relative cross sections for inelastic collisions from each since there is an interaction requirement in the trigger, and the typical DISC efficiency range.

The best fit parameters and the chisquared per degree of freedom for the six paramcter, four binomial fits to the distributions shown in Figures 10 and 11 (including all bins that contain data, typically ~32) are shown in Table III. The function used to fit the TRD plane count distribution for the events not tagged by the DISC as kaons on a normal data tape is of the form:

$$\begin{aligned} N_n &= N_{tot} \times C(48,n) \times (f_1 p_1^n (1-p_1)^{48-n} + (.507 - f_1) p_2^n (1-p_2)^{48-n} \\ &\quad + f_2 p_3^n (1-p_3)^{48-n} + (.493 - f_2) p_4^n (1-p_4)^{48-n}), \end{aligned}$$

where N_n is the number of events with n planes hit, f1 and f2 are the fractions of the events in the first or second peak, respectively, with average plane hit probability p_1 or p_3. The remaining two binomials have average plane hit probabilities p_2 and p_4. C(48,n) is the binomial coefficient for n out of 48 hits. The fraction of data in the first and second peaks has been changed from .507 and .493 to .980 and .020 for the DISC-tagged proton and kaon samples. The DISC-tagged pion sample could be adequately fit as a single peak composed of only two binomials, but a better fit was achieved by including a 1% fraction of kaons constrained to the plane probabilities derived from the kaon fit. Thus, the three starred parameters shown in the table for the pion fit were held fixed to the values determined in fitting the kaon peak in Figure 10c). The curves corresponding to these fits (solid lines) are superimposed on the distributions to allow bin by bin comparison. The dashed and dotted lines show the separate contribution from each of the two components. For charm data analysis, samples of pions or protons are selected by cutting above (for pions) or below (for protons) a chosen plane count. The efficiencies and contaminations are then determined using the fitting functions as was done for the DISC tagged data shown in Table II.

Table III - Results of Fits to the Data in Figures 10 and 11

Figure	f1	p1	p2	f2	p3	p4	χ^2/d.f.
10a)	.650	.056	.085	.004	.450	.245	.635
10b)	.008*	.089*	.132*	.201	.209	.308	1.59
10c)	.827	.089	.132	.006	.436	.285	.791
11	.387	.065	.118	.184	.344	.272	1.271

*These parameters were not allowed to float in the fit but were held fixed to the values for a 1% admixture of kaons using the parameters from the fit to 10c). This reduced χ^2 from 2.00/d.f. to the number shown.

Comparison of Data with Monte Carlo Predictions

A Monte Carlo program which can accurately predict the performance of a TRD for various choices of radiator material and detector gas composition is a valuable design tool. Thus, an important contribution to this report is confirmation that the programs used in the simulations of this detector correctly modeled its response. To determine this, the expected response of the detector to the incident pions on a typical positive beam data tape was predicted and compared to the data. The test distribution was created by using the measured hit probabilities for the protons on the same tape to estimate the signal due to ionization loss in the absence of TR and adding to this the Monte Carlo estimate for TR.

The way in which this was done can be explained by first referring to the distribution shown in Figure 11, although the distribution shown is not the same one that was used in the comparison. The events with plane counts less than 7 were assumed to have protons incident and the hit probability per event for each of the 48 planes in the detector was determined for these. The events with plane counts greater than 10 were assumed to have pions incident, and plane hit probabilities were calculated for them as well. These are shown as the lower and upper solid curves on Figure 12, respectively. The dashed curve shown on the figure is the simulated response of the

detector to pions, which is to be compared to the upper solid curve. The expected TR response was estimated using the calculated average number of TR photons radiated by the 200 12.7 μm foil radiator stack and detected in the 2-plane xenon chamber, 1.116. This was multiplied by the 83% efficiency to be above the electronics threshold measured in the source tests, which yields .926. A Poisson distribution with this average was then used as input to a program which used Monte Carlo techniques to predict the number of clusters detected per module. The calculated energy distribution was input as well, since the stopping point distribution depends on this. Since only one cluster per plane could be recorded in the latch, this was included in the modeling. If a plane did not record a hit due to TR, the possibility that it might register a hit due to ionization was accounted for by Monte Carlo sampling using the proton hit probability for that particular plane. It can be seen in the figure that the distribution made up in this way somewhat over-predicts the response of the front planes and under-predicts the response of the back planes. When the response of the two planes is summed, however, to allow comparison module by module, the data and predictions agree to within 10% for 20 of the 24 modules. The predicted average plane count for pions is 20 to be compared to the measured average of 18.8.

The data shown in Figure 11 were taken late in the data run after it was noticed that the chamber cathodes had suffered a considerable amount of damage due to the extremely high rates to which they had been exposed. The detector array was then raised about one inch to place an undamaged area into the beam and the gains were reduced to retard further dealuminization of the cathodes. The pion average plane count for the data shown in the figure is therefore somewhat lower than that of the data used in the above comparison.

Future Prospects

Figure 13 shows the predictions of the same Monte Carlo program for operation of the TRD in the 500 GeV/c negative beam for the follow-on experiment to E769, E791, which is taking data during the current Fixed

Target run at Fermilab. The beam has been assumed to be 98% pions and 2% kaons, which is the expected ratio at this energy[24]. Figure 13b) displays the low plane count region of Figure 13a) with a change of scale to demonstrate that the kaons can be well separated from the pions. The cathodes for the chambers have been rebuilt in preparation for E791 using aluminized mylar that has ten times the thickness of aluminum as on the originals ($\sim 1400\mathring{A}$) to enable operation for a longer period without a significant loss of performance. Also, the analog output circuits used to monitor the response of the on-board ^{55}Fe sources to establish gain uniformity from one chamber to the next during E769 were sampling edge wires of the chamber, and they therefore were not sensitive to the beam damage. These have been re-routed to sample wires which are in the beam area for E791 so that any degradation in performance will be evident immediately.

Summary

We have designed, built, and operated a transition radiation detector for use in differentiating beam particle species in a 250 GeV/c beam of charged hadrons. The detector operated in good agreement with predictions of a Monte Carlo program, and is providing valuable data for use in understanding the production of charmed particles by hadrons. It fulfilled the expected advantages of TRDs in such applications by imposing few constraints on the design of the beamline and, once operating conditions were established, by remaining stable with much less intervention than is usually required of beam Cerenkov counters or electrostatic or radio frequency beam separators.

Acknowledgements

The authors are deeply indebted to their collaborators on Fermilab Experiment E769 for their assistance with the installation, operation, and analysis of this device. The entire system was constructed by employees of the Fermilab Research Facilities Department, Technical Support Section,

and the Physics Department electronics shop. We express our gratitude for their dedicated effort.

*Work supported under NSF PHY-86-15287 and PHY-89-01274,
and DOE DE-AC02-76-ER00881-Task D and DE-AC02-76-CHO-3000.

References

[1] V.L. Ginzburg and I.M. Frank, Zh. Eksperim. Teor. Fiz. 16 (1946) 15.

[2] B. Dolgoshein, "Transition Radiation Detectors and Particle Identification", NIM A252 (1986) 137.

[3] J. A. Appel, "QCD: Photoproduction/Hadroproduction of Heavy Flavors: Fermilab E-691, E-769 and Beyond", Fermilab - CONF- 88/22, Feb. 1988. Invited talk given at Advanced Workshop on QCD Hard Hadronic Processes, St. Croix, Virgin Isl., Oct 8-13, 1987.

[4] M. Benot et al., "Cerenkov Counters for Particle Identification at High Energies", NIM 105 (1972) 431.

[5] H. Stroebele et al., "A Transition Radiation System for Identification of Pions in a 200–400 GeV Beam", submitted to NIM (1982).

[6] X. Artru et al., "Practical theory of the multilayered transition radiation detector", Phys. Rev. D12 (1975) 1289. See p. 1297 for a discussion of saturation.

[7] A. V. Kulikov et al.,"Performance of the E715 Transition Radiation Detector", talk given at the First Annual Meeting (New Series) of the Division of Particles and Fields of the American Physical Society, Santa Fe, New Mexico, Oct 31 - Nov 3, 1984. Published in the proceedings edited by T. Goldman and Michael Martin Nieto, World Scientific Publishing Co. Pte. Ltd.

[8] G. Barr et al., "The NA31 Transition Radiation Detector", IEEE Transactions on Nuclear Science 36 (1989) 66.

[9] M. Baake et al., "A Transition Radiation Detector for Kaon/Pion Separation", NIM A281 (1989) 325.

[10] For a recent review, see J. Appel, "Heavy Flavor Production in Fixed-Target Experiments", talk given at the Xth Int. Conf. on Physics in Collision, Durham, North Carolina, June 21-23, 1990, published in the

proceedings by Editions Frontieres and World Scientific, Gif-sur-Yvette and Singapore (1990), pp.85-103.

[11] J.R. Raab et al.,"Measurement of the D^o, D^+, and D_s^+ Lifetimes", Phys. Rev. **D37** (1988) 2391.

[12] C. Fabjan et al., "Practical Prototype of a Cluster-Counting Transition Radiation Detector", NIM 185 (1981) 119.

[13] T. Ludlam et al.,"Particle Identification by Electron Cluster Detection of Transition Radiation Photons", NIM 180 (1981) 413.

[14] H. Fenker, "A Standard Beam PWC for Fermilab", Fermilab - TM - 1179.

[15] J. C. Anjos et al, " P791 Continued Study of Heavy Flavors at TPL", a proposal to Fermilab March 7, 1988.

[16] See the data sheet on product code AMC2084, Amersham Laboratories, White Lion Road Amersham, Buckinghamshire, England, HP7 9ll.

[17] J. Fischer et al., "Lithium Transition Radiator and Xenon Detector System for Particle Identification at High Energies", NIM 127 (1975) 525.

[18] J. Cobb et al., "Transition Radiators for Electron Identification at the CERN ISR", NIM 140 (1977) 413.

[19] Michael L. Cherry, "Measurements of the Spectrum and Energy Dependence of X-ray Transition Radiation", Phys. Rev. D17 (1978) 2245.

[20] M. Clemen (representing the Helios collaboration), "The Helios Transition Radiation Detector", talk given at the "Symposium on Particle Identification at High Luminosity Hadron Colliders", Fermilab, April 5-7, 1989, published in the proceedings of the symposium edited by Treva Gourlay and Jorge Morfin, p. 339.

[21] J. Fischer et al., "Proportional Chambers for Very High Counting Rates Based on Gas Mixtures of CF_4 with Hydrocarbons", NIM A238

(1985) 249.

[22] R.J. Yarema et al., "A Surface Mount Amplifier-Shaper-Discriminator and Preamplifier for the Fermilab CDF Tracking Chambers", IEEE Transactions on Nuclear Science, Vol. 33, No. 1, February 1986.

[23] LeCroy Research Systems Corp., 700 Chestnut Ridge Road, Chestnut Ridge, New York 10977-6499.

[24] A. Malensek, Fermilab, private communication, Nov. 1988.

Figures

[1] Distribution of all events on a typical positive beam data tape to demonstrate the discrimination possible from the two detectors used in beam particle identification. The number of DISC phototubes hit is shown along one axis and the number of TRD chamber planes hit along the other. The peaks due to the three incident beam species are shown to be well-separated.

[2] Expected average number of TR photons detected per module of the TRD for an incident pion, kaon, or proton as a function of beam particle energy as calculated using the Monte Carlo program described in the text. The numbers have been multiplied by the measured efficiency of .83 for the signal to be above the electronics threshold. γ_{sat} has been determined using the formulae in Reference 5.

[3] Schematic of the PE5 beamline showing the placement of the two tagging detectors and the various beamline elements (not to scale).

[4] Schematic of one of the 24 TRD radiator-chamber assemblies labeled to show the significant design parameters.

[5] Photograph of one module of the TRD with its attached preamplifiers. The array of modules on the integrated system stand, which can be rolled in and out of the beamline, is seen in the background.

[6] Peak in the measured ADC pulse height spectrum (converted to millivolts) versus x-ray source energy in keV for the various sources used in the prototype tests at the nominal chamber operating voltage of 2650 volts.

[7] Average number of TR photons per keV produced and detected in one module of the TRD as a function of photon energy in keV for an incident 250 GeV pion or kaon as calculated using the Monte Carlo program. The three upper curves are for pions incident on 200-foil radiator stacks made from 10.2 μm (solid curve), 12.7 μm (dashed curved), and 17.8 μm (dotted curve) CH_2 foils, all with 180 μm He gaps. The lower curve is for kaons incident on a 200 foil stack made

from 12.7 μm foils (dash-dotted curve), which was the thickness used in the detector as built. The structure evident in the curve for the 17.8 μm foil set in the vicinity of 4 keV is due to the occurrence of an interference minimum there. (See the discussion in Section II.B. of Reference 6.) The energies of the various x-ray sources used in testing the prototype and the set value for the discriminator threshold on the ASD card (ASD THRESH) are shown on the abscissa to demonstrate their relationship to the spectrum expected to be produced by the radiator stack.

[8] The lower curve is the same curve as the dashed curve shown in Figure 7 but plotted on a log scale. This allows comparison to the upper curve, which is the number of photons produced in a single 12.7 μm CH_2 foil (multiplied by 200). This removes the effect of foil self-absorption. For the upper curve, there is also no requirement that the photons be detected in the xenon chamber planes. The severe attenuation at lower photon energies is the loss due to absorption in the foil stack. The loss at higher photon energies is caused by x-rays which escape from the chamber volume without being detected due to the lengthening of the mean free path for x-ray absorption with photon energy.

[9] Block diagram of the system electronics.

[10] TRD plane count distribution for samples of events tagged by the DISC to be a) protons, b) pions, and c) kaons. The pion and proton data are derived from special calibration runs. The kaon data are the DISC-tagged sample from a typical positive beam data tape. The curves shown are the best fits to these distributions using the methods described in the text. The parameters and the chisquared per degree of freedom for the fits are given in Table III.

[11] TRD plane count distribution for the events not identified by the DISC to be kaons from the same positive beam run as the DISC-tagged kaon sample shown in Figure 10c). The solid curve shown is the best fit to this distribution using four binomial functions as described in the text. The dotted and dashed curves show the separate contributions from

the protons and pions, respectively. See Table III for the parameters and chisquared per degree of freedom for the fit.

[12] Hit probability per event for each plane of the TRD for protons (lower solid curve) and pions (upper solid curve) for a positive beam data tape taken somewhat earlier in the data taking run when the TRD chamber gains set to the nominal operating voltage. The Monte Carlo predicted hit probabilities for pions for each plane calculated as described in the text are shown as the dashed curve for comparison to the data.

[13] TRD plane count distributions for pions (dashed curve) and kaons (solid curve) as predicted by the Monte Carlo for a 500 GeV beam incident are shown in a). b) is a detail of the low plane count region of a) shown on a different scale to demonstrate that the two species are expected to be well-separated. The relative beam fractions assumed are 98% pions and 2% kaons, which is the expected mix at this energy according to Reference 24.

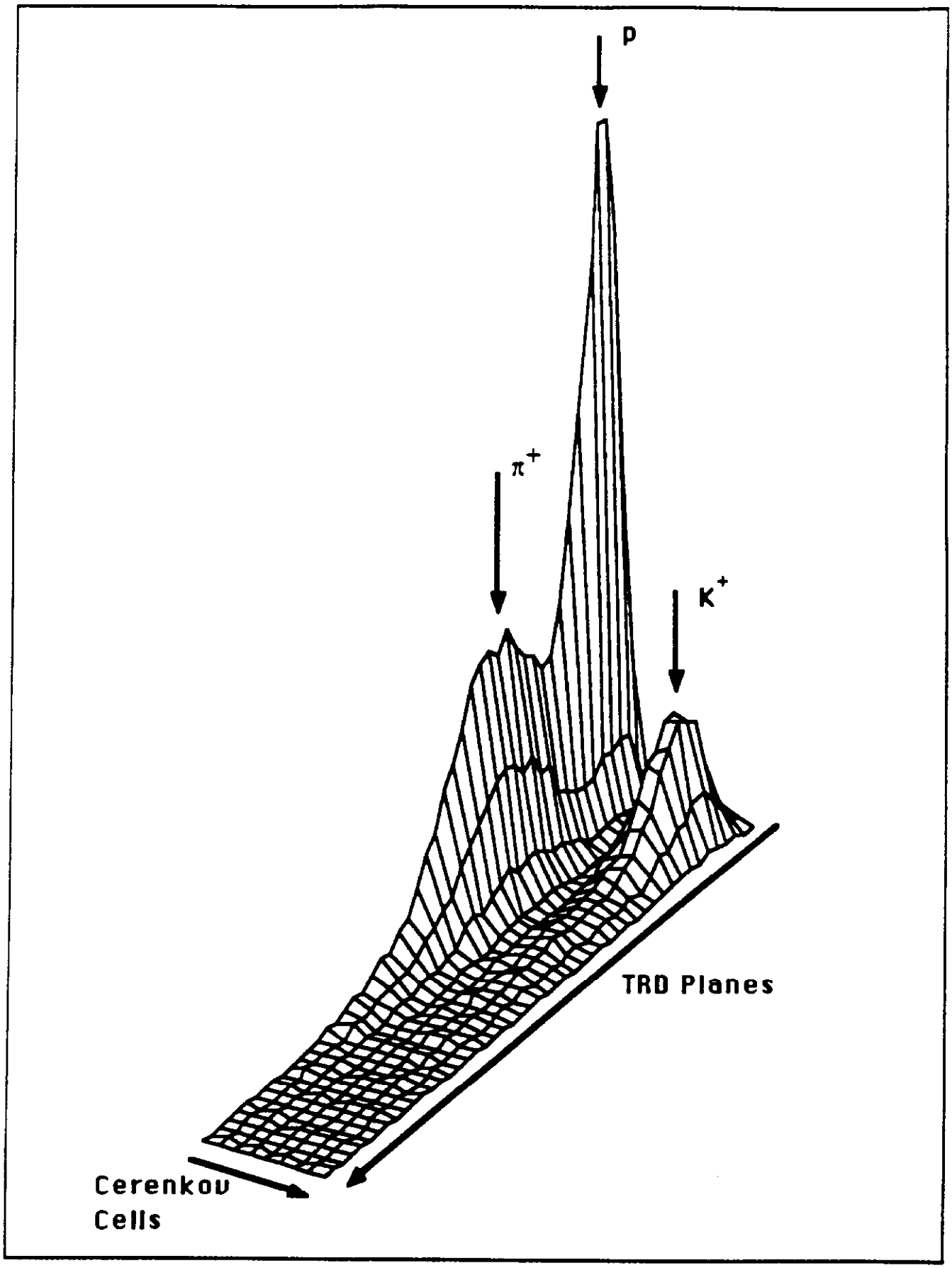

FIGURE 1

FIGURE 2

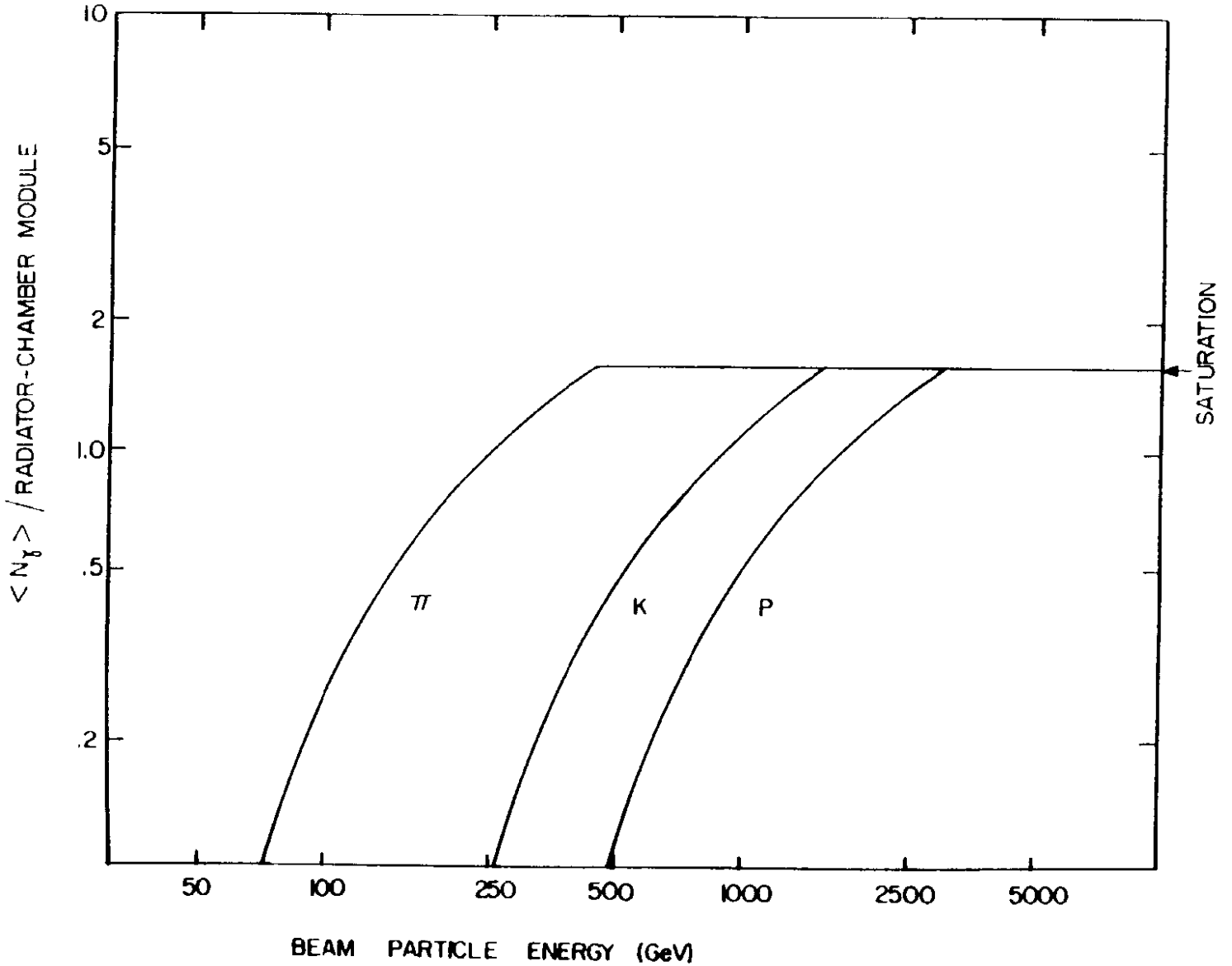
10
5
2
1.0
.5
.2
$< N_\gamma >$ / RADIATOR-CHAMBER MODULE
π
K
P
SATURATION
50
100
250
500
1000
2500
5000
BEAM PARTICLE ENERGY (GeV)

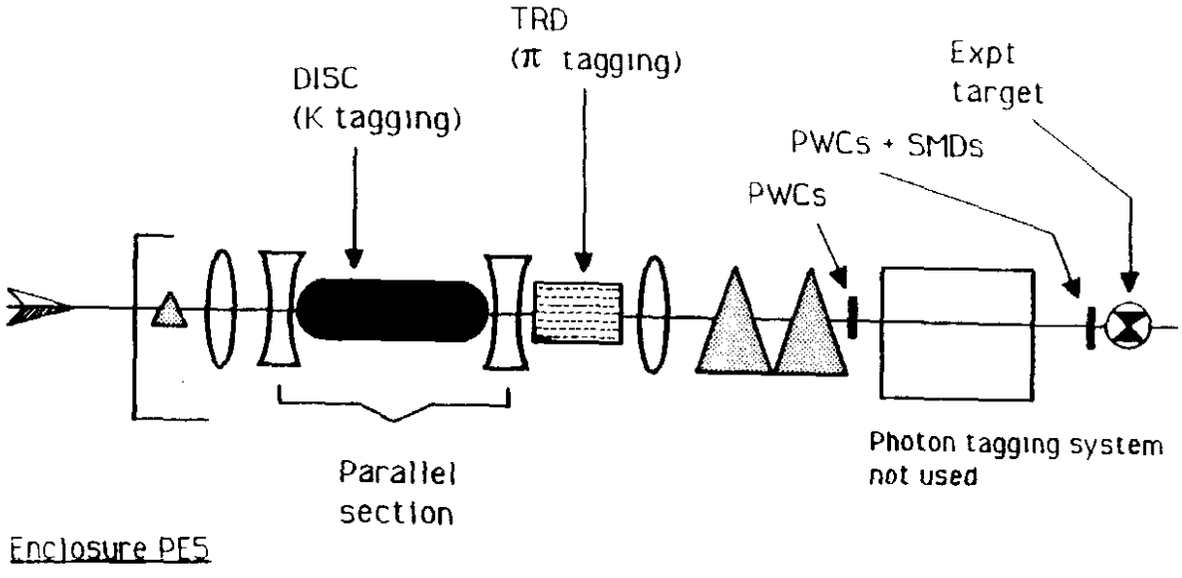
TRD
(π tagging)
DISC
(K tagging)
Expt
target
PWCs + SMDs
PWCs
Photon tagging system
not used
Parallel
section
Enclosure PE5

FIGURE 3

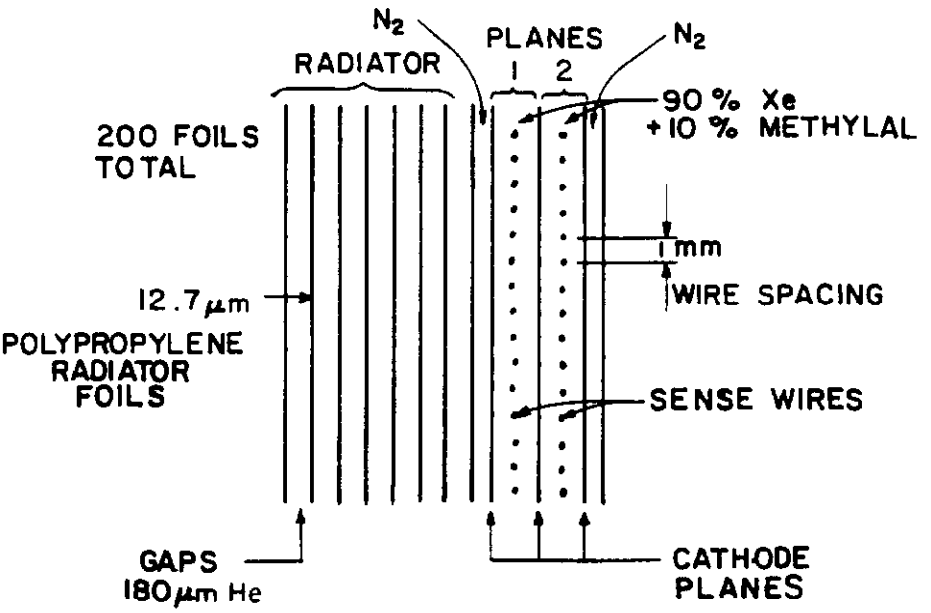
N_2
RADIATOR
PLANES
1
2
N_2
90 % Xe
+10 % METHYLAL
200 FOILS
TOTAL
1 mm
WIRE SPACING
12.7 μm
POLYPROPYLENE
RADIATOR
FOILS
SENSE WIRES
GAPS
180 μm He
CATHODE
PLANES

FIGURE 4

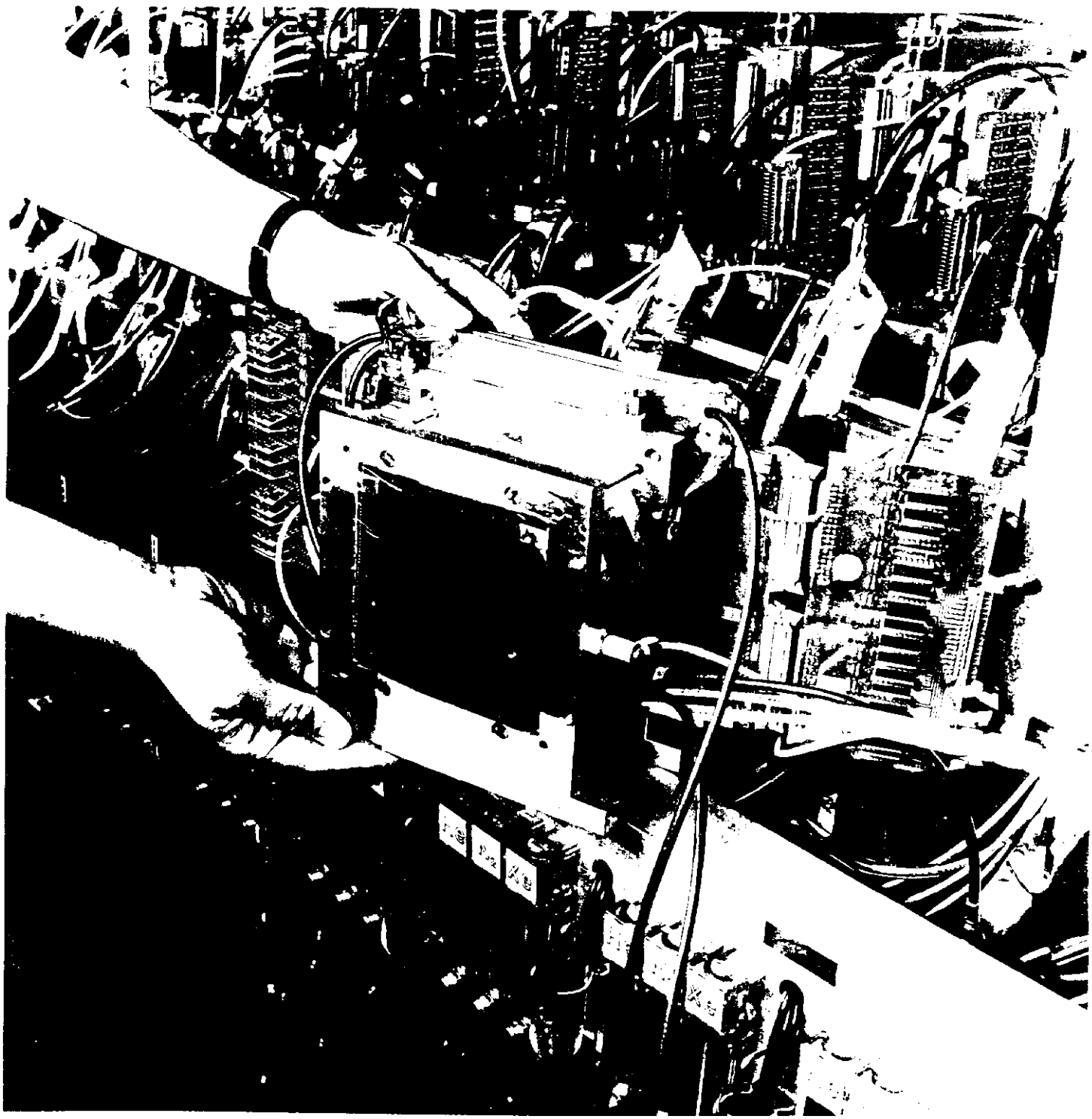

FIGURE 5

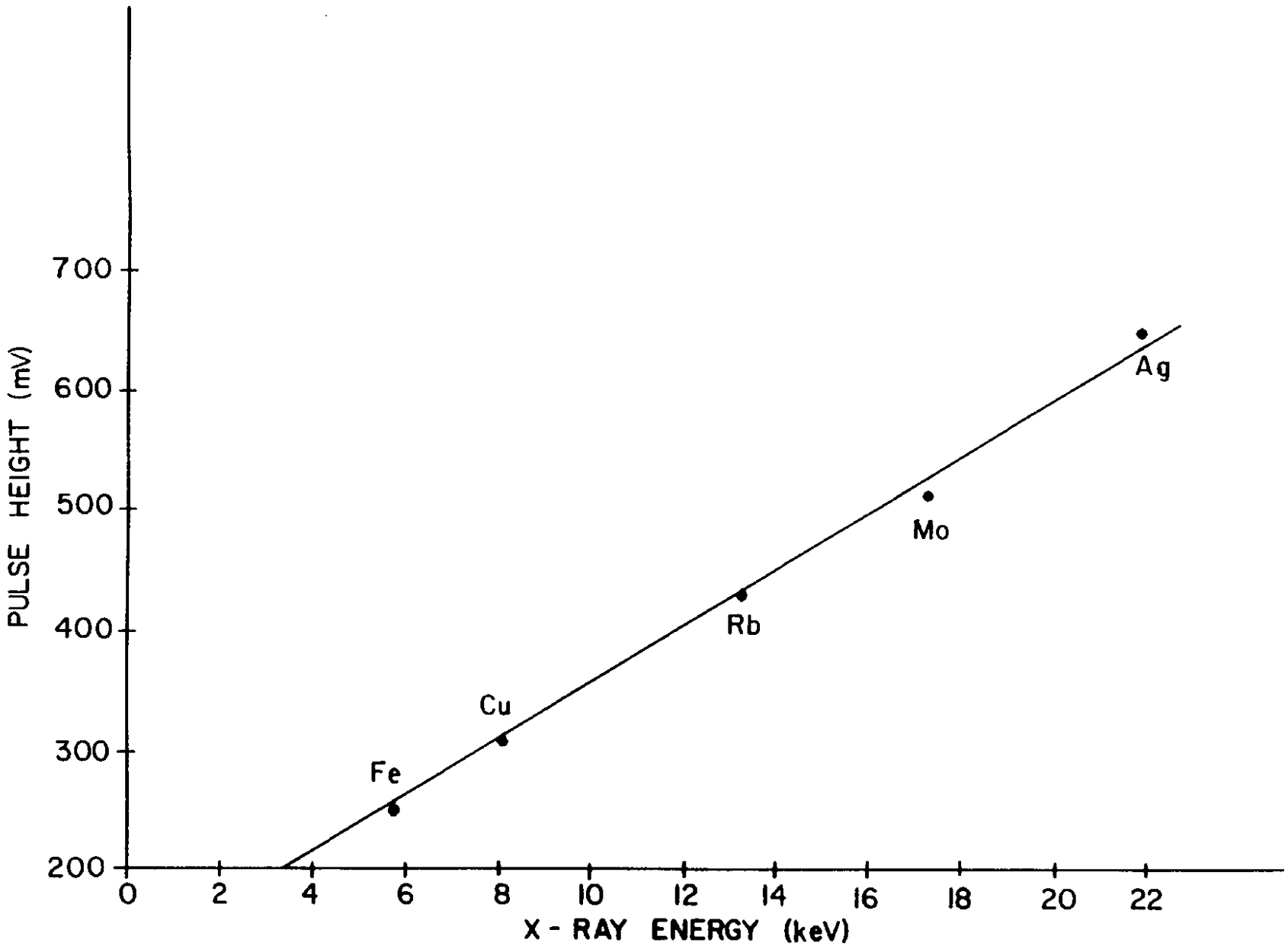
PULSE HEIGHT (mV)
700
600
500
400
300
200
0
2
4
6
8
10
12
14
16
18
20
22
X - RAY ENERGY (keV)
Fe
Cu
Rb
Mo
Ag

FIGURE 6

FIGURE 7

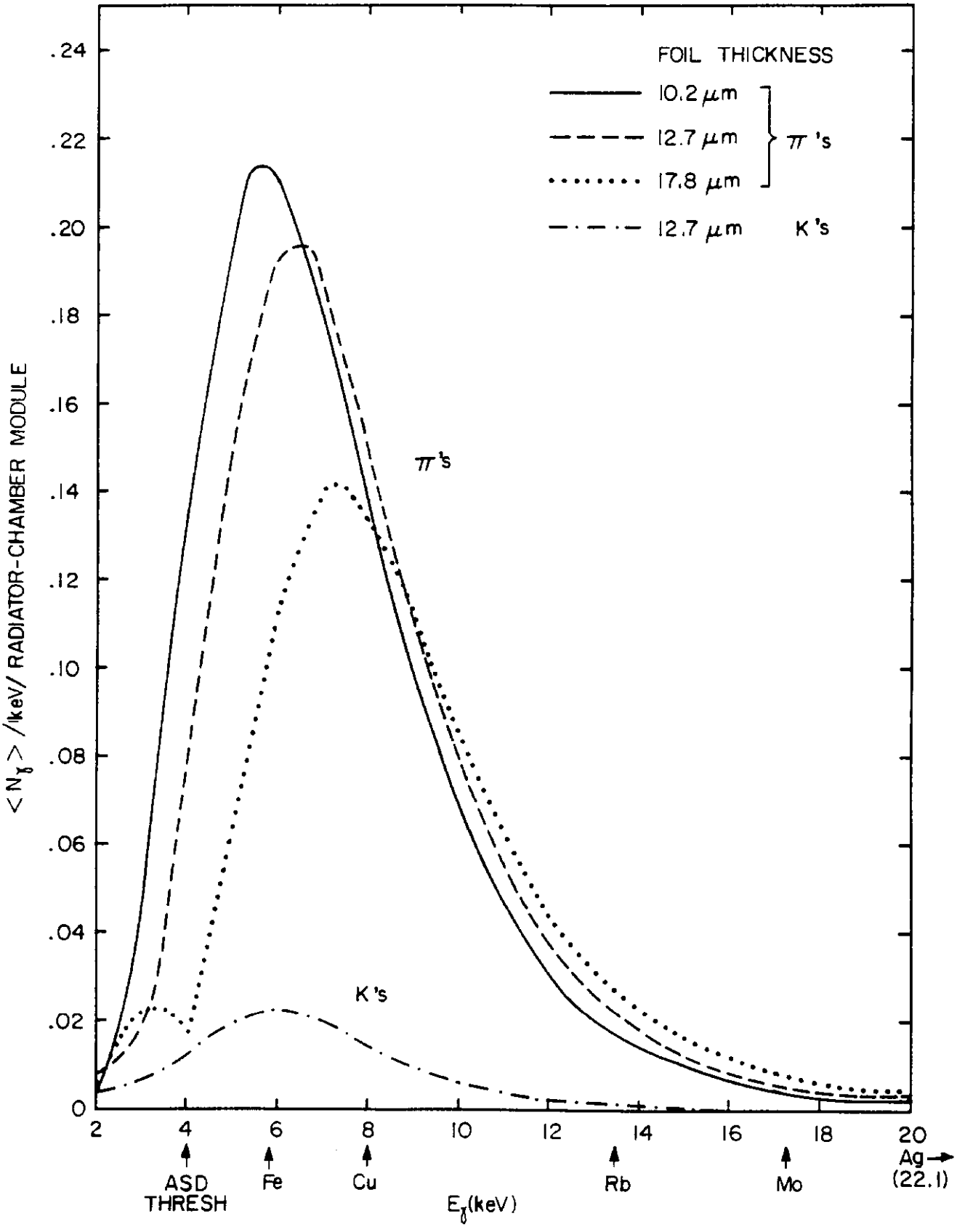
FOIL THICKNESS
10.2 μm
12.7 μm
17.8 μm
π 's
12.7 μm
K 's
π 's
K 's
< Nγ > /keV/ RADIATOR-CHAMBER MODULE
.24
.22
.20
.18
.16
.14
.12
.10
.08
.06
.04
.02
0
2
4
6
8
10
12
14
16
18
20
Ag (22.1)
ASD THRESH
Fe
Cu
Rb
Mo
Eγ(keV)

FIGURE 8

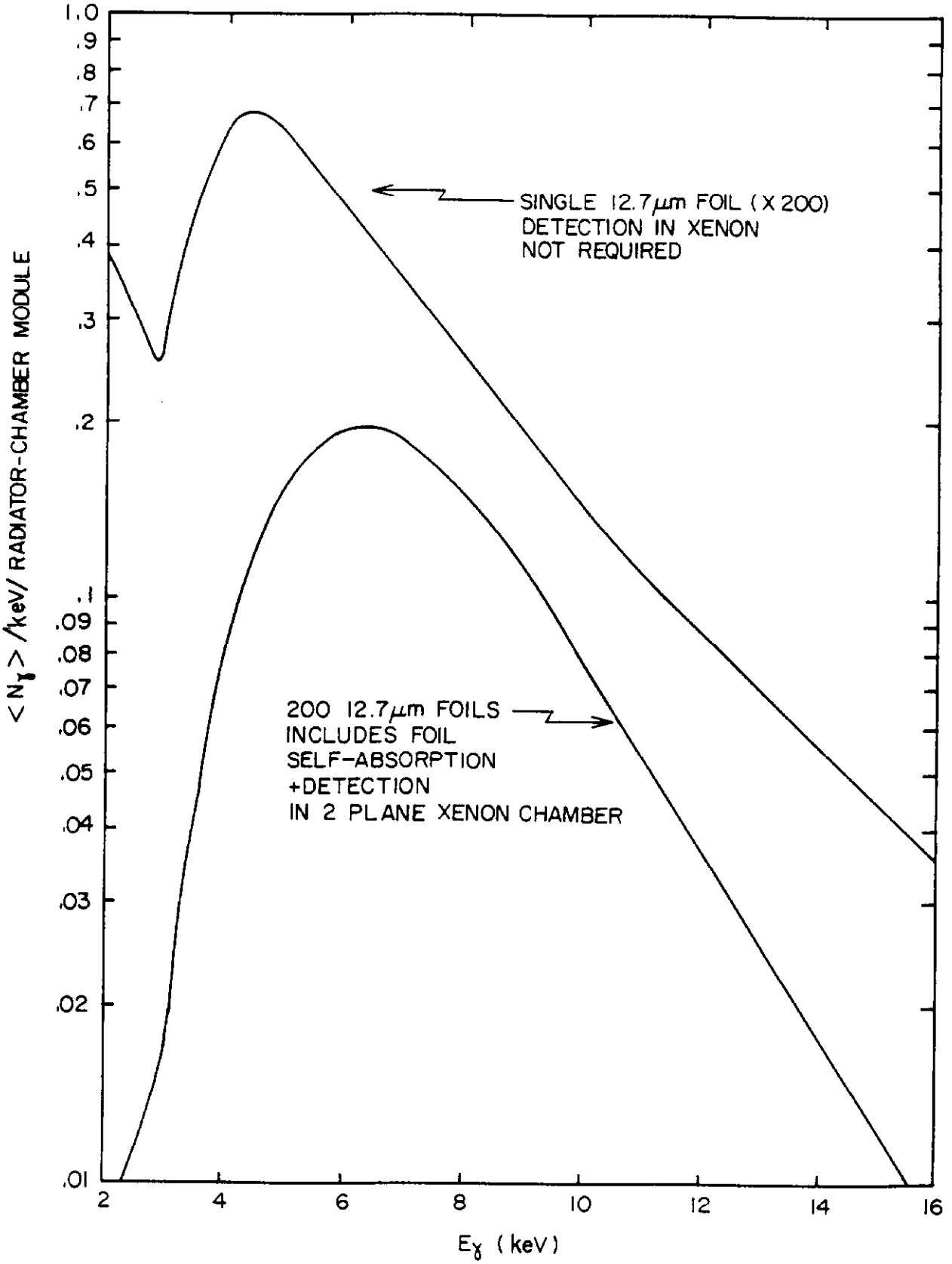
1.0
.9
.8
.7
.6
.5
.4
.3
.2
.1
.09
.08
.07
.06
.05
.04
.03
.02
.01
2
4
6
8
10
12
14
16
$\langle N_\gamma \rangle$ /keV/ RADIATOR-CHAMBER MODULE
E_γ (keV)
SINGLE 12.7μm FOIL (X 200)
DETECTION IN XENON
NOT REQUIRED
200 12.7μm FOILS
INCLUDES FOIL
SELF-ABSORPTION
+DETECTION
IN 2 PLANE XENON CHAMBER

TRD ELECTRONICS

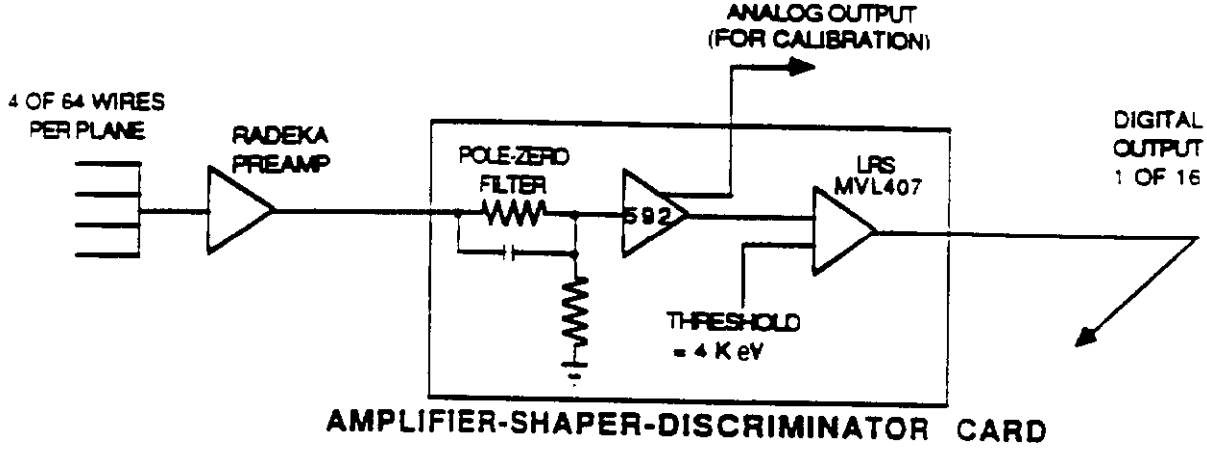

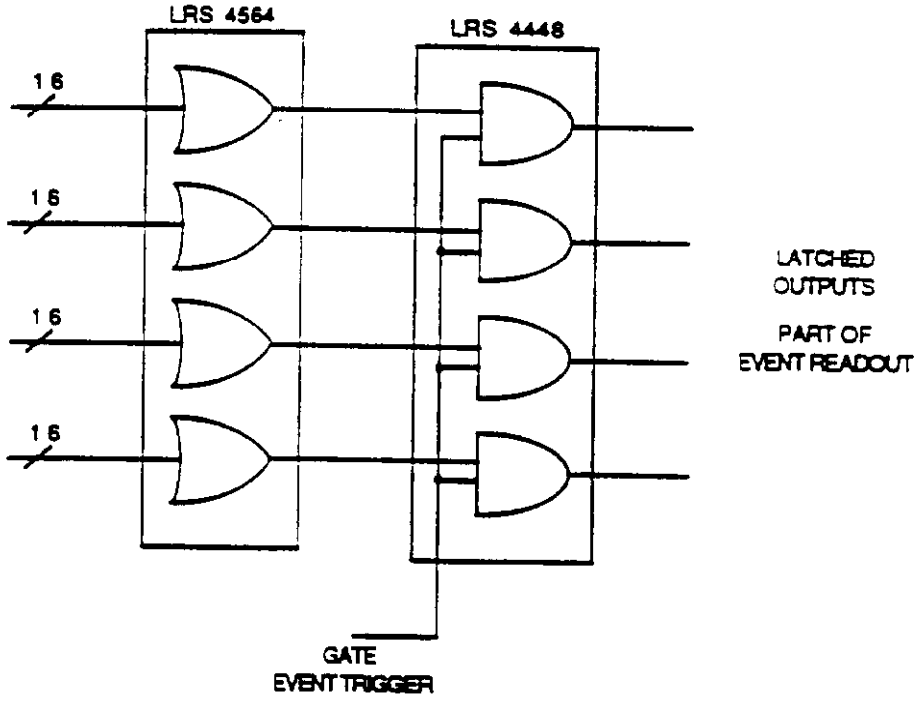

FIGURE 9

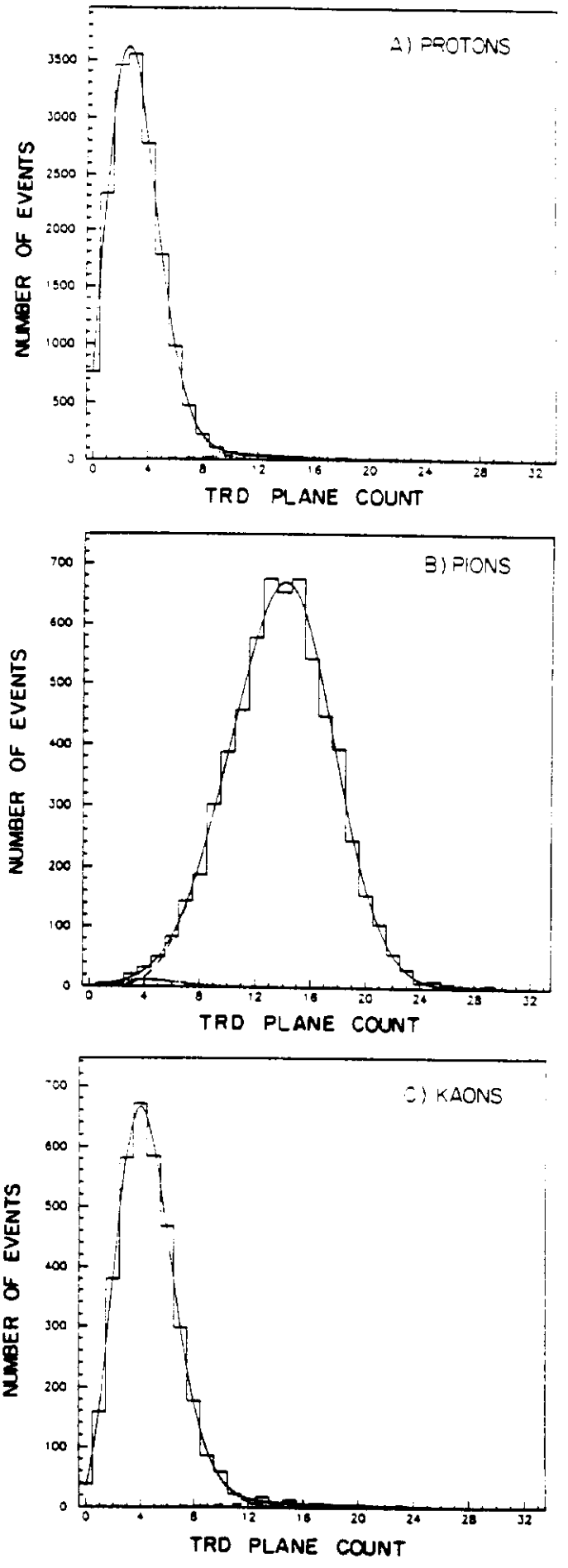
A) PROTONS
NUMBER OF EVENTS
TRD PLANE COUNT
B) PIONS
NUMBER OF EVENTS
TRD PLANE COUNT
C) KAONS
NUMBER OF EVENTS
TRD PLANE COUNT

FIGURE 10

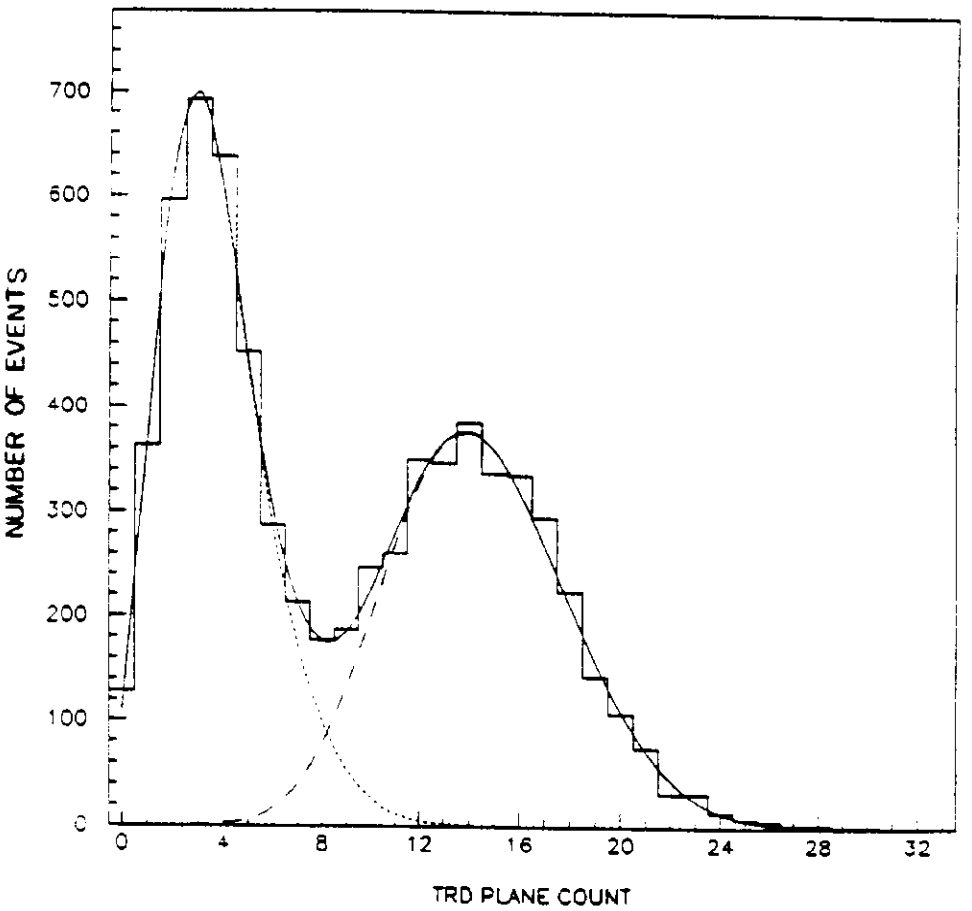
NUMBER OF EVENTS
700
600
500
400
300
200
100
0
0
4
8
12
16
20
24
28
32
TRD PLANE COUNT

FIGURE 11

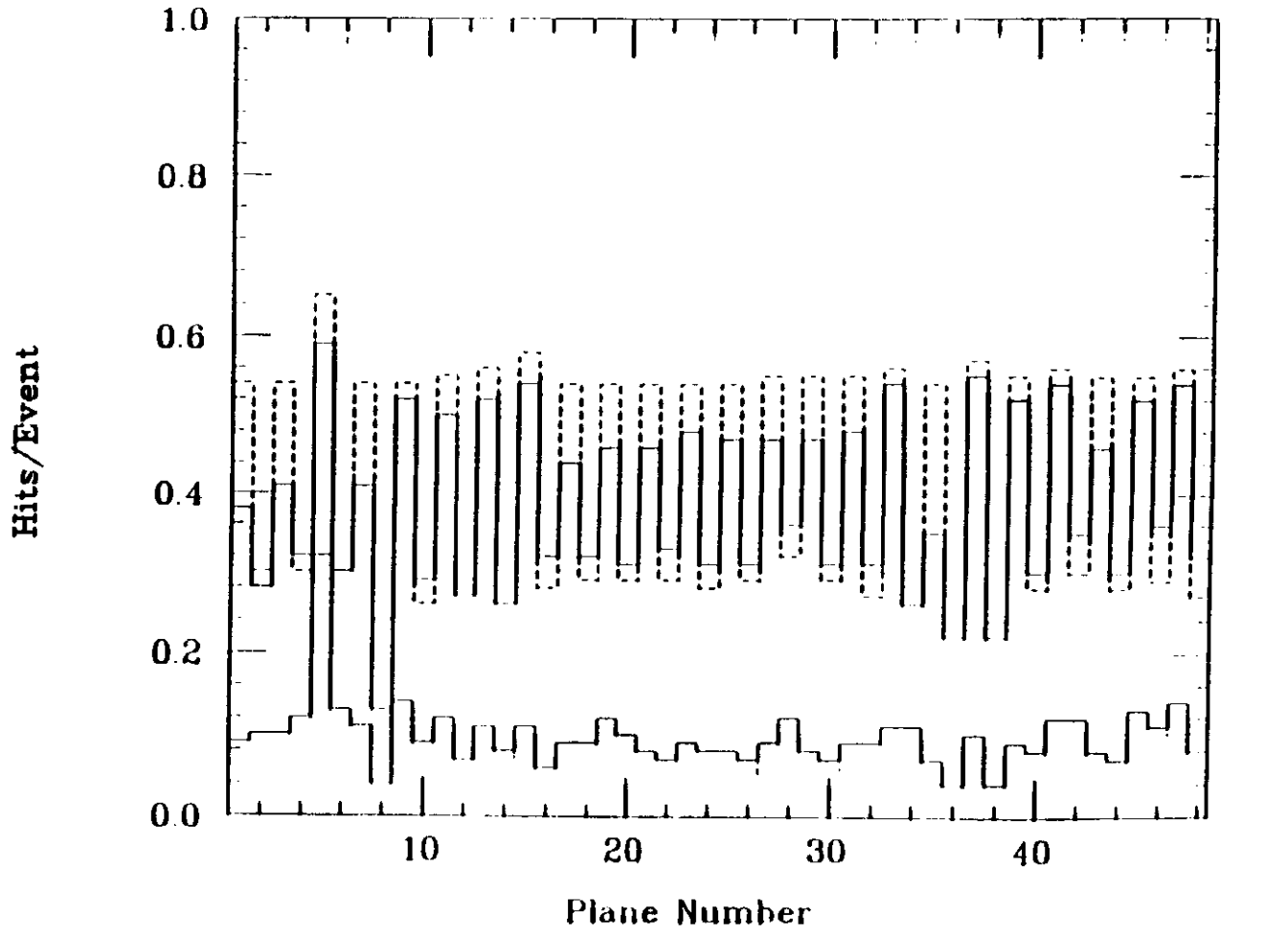
Plane by Plane Comparison of Data and Monte Carlo
1.0
0.8
0.6
0.4
0.2
0.0
Hits/Event
10
20
30
40
Plane Number

FIGURE 12

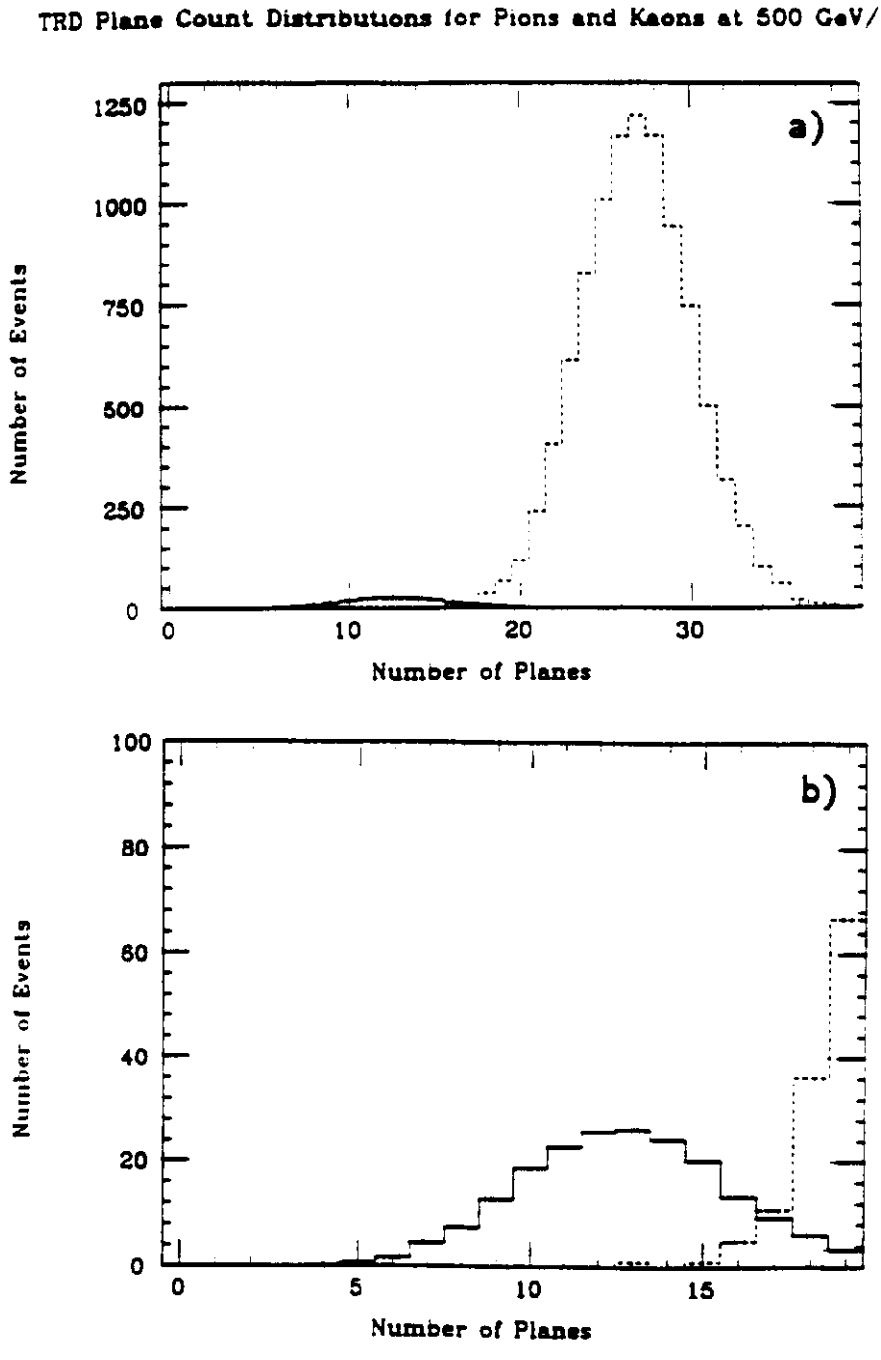
TRD Plane Count Distributions for Pions and Kaons at 500 GeV/c
a)
Number of Events
Number of Planes
1250
1000
750
500
250
0
0
10
20
30
b)
Number of Events
Number of Planes
100
80
60
40
20
0
0
5
10
15

FIGURE 13